

# Nonlinear wave dynamics near phase transition in $\mathcal{PT}$ -symmetric localized potentials

Sean Nixon and Jianke Yang

*Department of Mathematics and Statistics, University of Vermont, Burlington, VT 05401, USA*

Nonlinear wave propagation in parity-time ( $\mathcal{PT}$ ) symmetric localized potentials is investigated analytically near a phase-transition point where a pair of real eigenvalues of the potential coalesce and bifurcate into the complex plane. Necessary conditions for phase transition to occur are derived based on a generalization of the Krein signature. Using multi-scale perturbation analysis, a reduced nonlinear ODE model is derived for the amplitude of localized solutions near phase transition. Above phase transition, this ODE model predicts a family of stable solitons not bifurcating from linear (infinitesimal) modes under a certain sign of nonlinearity. In addition, it predicts periodically-oscillating nonlinear modes away from solitons. Under the opposite sign of nonlinearity, it predicts unbounded growth of solutions. Below phase transition, solution dynamics is predicted as well. All analytical results are compared to direct computations of the full system and good agreement is observed.

## I. INTRODUCTION

Parity-time ( $\mathcal{PT}$ ) symmetric systems started out from an observation in non-Hermitian quantum mechanics, where a complex but  $\mathcal{PT}$ -symmetric potential could possess all-real spectrum [1]. This concept later spread out to optics, Bose-Einstein condensation, mechanical systems, electric circuits and many other fields, where a judicious balancing of gain and loss constitutes a  $\mathcal{PT}$ -symmetric system which can admit all-real linear spectrum [2–12]. For example, in optics an even refractive index profile together with an odd gain-loss landscape yields a  $\mathcal{PT}$ -symmetric system. A common phenomenon in linear  $\mathcal{PT}$ -symmetric systems is phase transition (also known as  $\mathcal{PT}$ -symmetry breaking), where pairs of real eigenvalues collide and then bifurcate to the complex plane when the magnitude of gain and loss is above a certain threshold [1, 6, 13–15]. This phase transition has been observed experimentally in a wide range of physical systems [3–5, 7, 10, 11]. When nonlinearity is introduced into  $\mathcal{PT}$  systems, the interplay between nonlinearity and  $\mathcal{PT}$  symmetry gives rise to additional novel properties such as the existence of continuous families of stationary nonlinear modes, stabilization of nonlinear modes above phase transition, and symmetry breaking of nonlinear modes [6, 14–22]. These findings reveal that  $\mathcal{PT}$ -symmetric systems break the boundaries between traditional conservative and dissipative systems and open new exciting research territories. Practical applications of  $\mathcal{PT}$  systems are starting to emerge as well, such as recent demonstrations of  $\mathcal{PT}$ -symmetric micro-ring lasers and unidirectional  $\mathcal{PT}$  metamaterials [9, 12, 17, 23].

An important feature of  $\mathcal{PT}$ -symmetric systems is phase transition, where the linear spectrum changes from all-real to partially-complex and infinitesimal waves change from stable to unstable. At phase transition, a pair of real eigenvalues coalesce and form an exceptional point with a non-diagonal Jordan block (i.e., with the algebraic multiplicity higher than the geometric multiplicity). Phase transition is a distinct linear property of  $\mathcal{PT}$ -symmetric systems, and it is at the heart of many proposed applications such as  $\mathcal{PT}$ -symmetric micro-ring

lasers and unidirectional  $\mathcal{PT}$  metamaterials [9, 12].

When nonlinearity is present (such as if the wave amplitude is not small), the interplay between phase transition and nonlinearity is a fascinating subject. This interplay was previously studied for periodic  $\mathcal{PT}$ -symmetric potentials in [21, 24, 25], where novel behaviors such as wave-blowup and oscillating bound states were reported below phase transition. In addition, stable nonlinear Bloch modes were reported above phase transition because nonlinearity transforms the effective potential from above to below phase transition [21]. However, in periodic potentials above phase transition, the presence of unstable infinitely extended linear modes makes the zero background unstable, which excludes the possibility of stable spatially-localized coherent structures. In localized potentials, will the situation be different?

In this article we study nonlinear wave behaviors in localized  $\mathcal{PT}$ -symmetric potentials near phase transition. Unlike periodic potentials, the instability of linear modes above phase transition is limited to the area around the localized potential. In this case, the addition of nonlinearity can balance against gain and loss making stable spatially-localized coherent structures, such as solitons and oscillating bound states, possible above phase transition. Mathematically we explain this phenomenon by a multi-scale perturbation analysis, where a reduced nonlinear ODE model is derived for the amplitude of localized solutions near phase transition. Above phase transition, this ODE model predicts a family of stable solitons not bifurcating from linear (infinitesimal) modes under a certain sign of nonlinearity. In addition, it predicts persistent oscillating nonlinear modes away from solitons. Under the opposite sign of nonlinearity, it predicts unbounded growth of solutions. Similarly, solution dynamics below phase transition is predicted as well. All these predictions are verified in the full PDE system. In addition to these nonlinear dynamics, we also derive a necessary condition for phase transition to occur at an exceptional point in the linear  $\mathcal{PT}$  system by a generalization of the Krein signature, namely, phase transition from a collision of two real eigenvalues is possible only when the two eigenvalues have opposite  $\mathcal{PT}$ -Krein signatures.

## II. PRELIMINARIES

The mathematical model we consider in this article is the following potential NLS equation

$$i\psi_z + \psi_{xx} + V(x; \epsilon)\psi + \sigma|\psi|^2\psi = 0, \quad (2.1)$$

where  $V(x; \epsilon)$  is a  $\mathcal{PT}$ -symmetric complex potential, i.e.,

$$V^*(-x; \epsilon) = V(x; \epsilon), \quad (2.2)$$

parameterized by  $\epsilon$  which controls the gain-loss strength,  $\sigma = \pm 1$  is the sign of nonlinearity, and the superscript ‘\*’ represents complex conjugation. This model governs nonlinear light propagation in an optical medium with gain and loss [14] as well as dynamics of Bose-Einstein condensates in a double-well potential with atoms injected into one well and removed from the other well [8]. Without loss of generality, we assume phase transition occurs at  $\epsilon = 0$ , where a pair of real eigenvalues of the potential coalesce and form an exceptional point, and we will analyze the solution dynamics in Eq. (2.1) near this exceptional point, i.e., when  $|\epsilon| \ll 1$ .

The analysis to be developed applies to all localized  $\mathcal{PT}$ -symmetric potentials near phase transition. To illustrate these analytical results and compare them with direct numerics of the full model (2.1), we will use a concrete example — the so-called Scarff II potential

$$V = V_R \text{sech}^2(x) + iW_0 \text{sech}(x) \tanh(x), \quad (2.3)$$

where  $V_R, W_0$  are real parameters. For this potential, phase transition occurs at  $W_0 = V_R + 1/4$  [13], and solitons as well as robust oscillating solutions were reported numerically below phase transition in [14, 26–28].

## III. $\mathcal{PT}$ -KREIN SIGNATURE AND A NECESSARY CONDITION FOR PHASE TRANSITION

We begin by studying the general linear eigenvalue problem

$$L(x; \epsilon)u = -\mu u, \quad (3.1)$$

where  $L$  is a  $\mathcal{PT}$ -symmetric linear operator parameterized by  $\epsilon$ , i.e.,

$$L^*(-x; \epsilon) = L(x; \epsilon), \quad (3.2)$$

and  $\mu$  is an eigenvalue. We wish to consider the phase-transition process by which the spectrum of  $L$  changes from all-real to partially-complex. This phase transition occurs when a pair of real eigenvalues collide and then bifurcate into the complex plane. It is important to recognize that not any two real eigenvalues can turn complex upon collision. This is analogous to the linear stability of equilibria in Hamiltonian systems, where not just any two purely imaginary eigenvalues upon collision

can bifurcate off the imaginary axis and create linear instability [29–31]. Then the question we address is: under what conditions can a pair of real eigenvalues of  $L$  induce phase transition upon collision?

For the potential NLS equation (2.1), when one looks for linear eigenmodes  $\psi = u(x)e^{-i\mu z}$ , the eigenvalue problem (3.1) will be obtained with

$$L = \partial_{xx} + V(x; \epsilon), \quad (3.3)$$

which is  $\mathcal{PT}$ -symmetric. However, in this section we will consider the eigenvalue problem (3.1) for general  $\mathcal{PT}$ -symmetric operators, not just (3.3).

First we make some elementary observations. Since the operator  $L$  is  $\mathcal{PT}$ -symmetric, any complex eigenvalues must come in conjugate pairs, i.e., if  $[\mu, u(x)]$  is an eigenmode, then so is  $[\mu^*, u^*(-x)]$ . If  $\mu$  is a simple real eigenvalue, then its eigenfunction  $u(x)$  can be made  $\mathcal{PT}$ -symmetric by scaling.

We start the analysis by introducing a sesquilinear  $\mathcal{PT}$ -product

$$\langle f, g \rangle_{\mathcal{PT}} \equiv \int_{-\infty}^{\infty} f^*(-x)g(x)dx, \quad (3.4)$$

which naturally satisfies the symmetry condition

$$\langle g, f \rangle_{\mathcal{PT}} = \langle f, g \rangle_{\mathcal{PT}}^*. \quad (3.5)$$

Thus for any complex function  $f(x)$ ,  $\langle f, f \rangle_{\mathcal{PT}}$  is real and invariant under a gauge transformation  $f(x) \rightarrow f(x)e^{i\theta}$ , where  $\theta$  is a real constant. In addition, under this  $\mathcal{PT}$ -product the  $\mathcal{PT}$ -symmetric operator  $L$  is “self-adjoint”, i.e.,

$$\langle Lf, g \rangle_{\mathcal{PT}} = \langle f, Lg \rangle_{\mathcal{PT}}. \quad (3.6)$$

For an eigenmode  $[\mu, u(x)]$  of (3.3) with a simple real eigenvalue  $\mu$  we define its  $\mathcal{PT}$ -Krein signature as

$$S(\mu) = \text{sgn} [\langle u, u \rangle_{\mathcal{PT}}]. \quad (3.7)$$

Here  $\langle u, u \rangle_{\mathcal{PT}} \neq 0$ , because  $u(x)$  can be made  $\mathcal{PT}$ -symmetric, i.e.,  $u^*(-x) = u(x)$ , so  $\langle u, u \rangle_{\mathcal{PT}} = \int_{-\infty}^{\infty} u^2 dx$ , which is nonzero since it is the Fredholm condition for the generalized-eigenfunction equation  $(L + \mu)u_g = u$  not to admit a solution in view that  $u^*(x)$  is in the kernel of the adjoint operator  $L^* + \mu$ . Thus the  $\mathcal{PT}$ -Krein signature of a simple real eigenvalue is always positive or negative. In addition, this signature cannot change under continuous variation of the parameter  $\epsilon$  unless pairs of such eigenvalues collide.

The main result of this section is that when two such eigenvalues collide, a necessary condition for complex-eigenvalue bifurcation is the two real eigenvalues have opposite  $\mathcal{PT}$ -Krein signatures. This result extends an analogous one in Hamiltonian systems to  $\mathcal{PT}$ -symmetric systems [29, 31].

We first present three lemmas.

**Lemma 1** Let  $u_1(x)$  and  $u_2(x)$  be two eigenfunctions of the  $\mathcal{PT}$ -symmetric operator  $L$  with real eigenvalues  $\mu_1$  and  $\mu_2$  respectively. If  $\mu_1 \neq \mu_2$  then  $\langle u_1, u_2 \rangle_{\mathcal{PT}} = 0$ .

**Proof** Using the “self-adjoint” property (3.6) we have

$$\langle u_1, Lu_2 \rangle_{\mathcal{PT}} = \langle Lu_1, u_2 \rangle_{\mathcal{PT}}.$$

Then using the fact that  $u_1$  and  $u_2$  are eigenfunctions, we can calculate the left and right sides of the above equation as

$$\langle u_1, Lu_2 \rangle_{\mathcal{PT}} = -\mu_2 \langle u_1, u_2 \rangle_{\mathcal{PT}},$$

and

$$\langle Lu_1, u_2 \rangle_{\mathcal{PT}} = -\mu_1 \langle u_1, u_2 \rangle_{\mathcal{PT}}.$$

Thus if  $\mu_1 \neq \mu_2$  then  $\langle u_1, u_2 \rangle_{\mathcal{PT}} = 0$ .  $\square$

**Lemma 2** Let  $u(x)$  be an eigenfunction of the  $\mathcal{PT}$ -symmetric operator  $L$  with a complex eigenvalue  $\mu$ . Then  $\langle u, u \rangle_{\mathcal{PT}} = 0$ .

**Proof** From Eq. (3.6) we have  $\langle u, Lu \rangle_{\mathcal{PT}} = \langle Lu, u \rangle_{\mathcal{PT}}$ . Calculating the two sides of this equation we get

$$(\mu - \mu^*) \langle u, u \rangle_{\mathcal{PT}} = 0.$$

Thus if  $\mu$  is complex, then  $\langle u, u \rangle_{\mathcal{PT}} = 0$ .  $\square$

**Lemma 3** Let  $\{e_j\}$  be a basis for an  $N$ -dimensional functional subspace and  $f = \sum_{j=1}^N c_j e_j$ . Then

$$\langle f, f \rangle_{\mathcal{PT}} = c^H M c,$$

where  $M$  is a  $N \times N$  Hermitian matrix with elements given by

$$M_{ij} = \langle e_i, e_j \rangle_{\mathcal{PT}}, \quad (3.8)$$

and the superscript ‘ $H$ ’ represents the Hermitian of a vector.

**Proof** Substituting the  $f$  expression into  $\langle f, f \rangle_{\mathcal{PT}}$  and utilizing the linearity of the  $\mathcal{PT}$ -product, this lemma can be readily proved. The Hermiticity of  $M$  comes directly from relations (3.5) and (3.6).  $\square$

Now we present the main result of this section.

**Theorem 4** Let  $L$  be a  $\mathcal{PT}$ -symmetric operator parameterized by  $\epsilon$ . If a pair of simple real eigenvalues of  $L$  collide and bifurcate into the complex plane at  $\epsilon = 0$ , then before the bifurcation the two real eigenvalues must have opposite  $\mathcal{PT}$ -Krein signatures.

**Proof** Let  $u_1(x)$  and  $u_2(x)$  be two eigenfunctions of  $L$  with eigenvalues  $\mu_1$  and  $\mu_2$  respectively; when  $\epsilon < 0$ ,  $\mu_1$  and  $\mu_2$  are simple real with  $\mu_1 \neq \mu_2$ , and when  $\epsilon > 0$ ,  $\mu_1$  and  $\mu_2$  are complex with  $\mu_1 = \mu_2^*$ . We analyze the

quadratic form  $\langle f, f \rangle_{\mathcal{PT}}$  restricted to the subspace  $S = \text{span}(u_1, u_2)$  by looking at the dual matrix  $M$ .

When  $\epsilon > 0$  and  $\mu_1 = \mu_2^*$ , we see easily by Lemma 2 that

$$M_{\epsilon > 0} = \begin{bmatrix} 0 & b \\ b^* & 0 \end{bmatrix}, \quad (3.9)$$

where  $b = \langle u_1, u_2 \rangle_{\mathcal{PT}}$ . In this case,  $u_1(x) = u_2^*(-x)$ , thus

$$b = \langle u_2^*(-x), u_2(x) \rangle_{\mathcal{PT}} = \int_{-\infty}^{\infty} u_2^2(x) dx,$$

which is nonzero because for a simple eigenvalue  $\mu_2$ ,  $\int_{-\infty}^{\infty} u_2^2 dx \neq 0$  is the Fredholm condition for non-existence of a generalized eigenfunction [see earlier text below Eq. (3.7)]. This means  $M$  has a pair of real eigenvalues of opposite sign and is thus indefinite.

Likewise, for  $\epsilon < 0$ , since  $\mu_1$  and  $\mu_2$  are strictly real, then in view of Lemma 1,

$$M_{\epsilon < 0} = \begin{bmatrix} a_1 & 0 \\ 0 & a_2 \end{bmatrix}, \quad (3.10)$$

where  $a_1 = \langle u_1, u_1 \rangle_{\mathcal{PT}}$  and  $a_2 = \langle u_2, u_2 \rangle_{\mathcal{PT}}$  have the signs of the  $\mathcal{PT}$ -Krein signatures for  $\mu_1$  and  $\mu_2$  respectively.

At  $\epsilon = 0$  the two eigenvalues collide, and  $\mu_1 = \mu_2 = \mu_0$ . There are two cases here. The first case is where  $L$  has two eigenfunctions  $u_1$  and  $u_2$  at  $\mu_0$ , i.e.,  $L$  has a diagonal Jordan block. In this case,  $\langle u_k, u_k \rangle_{\mathcal{PT}} \neq 0$  ( $k = 1, 2$ ), and we can always choose the basis  $\{u_1, u_2\}$  so that  $\langle u_1, u_2 \rangle_{\mathcal{PT}} = 0$ , thus the operator  $M_{\epsilon=0}$  has the same structure as (3.10). The second case is where  $L$  has a single eigenfunction  $u_0$  at  $\mu_0$ , i.e.,  $L$  has a non-diagonal Jordan block. In this case, the subspace  $S$  reduces to  $S = \text{span}(u_0, u_g)$ , where  $u_g$  is the generalized eigenfunction satisfying

$$(\mu_0 + L)u_g = u_0.$$

Taking the  $\mathcal{PT}$ -product of this equation with  $u_0$  and recalling (3.6), i.e., applying the Fredholm condition, we get  $\langle u_0, u_0 \rangle_{\mathcal{PT}} = 0$ , thus

$$M_{\epsilon=0} = \begin{bmatrix} 0 & c_1 \\ c_1^* & c_2 \end{bmatrix}, \quad (3.11)$$

where  $c_1 = \langle u_0, u_g \rangle_{\mathcal{PT}}$  and  $c_2 = \langle u_g, u_g \rangle_{\mathcal{PT}}$ . Note that  $c_1 \neq 0$  since it is the Fredholm condition for eigenvalue  $\mu_0$  not to have a second generalized eigenfunction. Then  $\det(M_{\epsilon=0}) < 0$ , hence  $M_{\epsilon=0}$  has a pair of real eigenvalues of opposite sign and is indefinite.

Since  $M$  is indefinite for  $\epsilon > 0$  and this indefiniteness is continuous across the bifurcation point  $\epsilon = 0$ , we see that  $M$  for  $\epsilon < 0$  must also be indefinite, which directly implies that real eigenvalues  $\mu_1$  and  $\mu_2$  before bifurcation must have opposite  $\mathcal{PT}$ -Krein signatures.  $\square$

Now we use an example to illustrate this theorem. In the Scarff-II potential (2.3), we fix  $V_R = 5$  and vary the

gain-loss coefficient  $W_0$ . The linear spectra for various  $W_0$  values are displayed in Fig. 1. It is seen that phase transition occurs at  $W_0 = 5.25$ , where a pair of simple real eigenvalues coalesce and form an exceptional point, which then turns complex when  $W_0 > 5.25$ . We have calculated the  $\mathcal{PT}$ -Krein signatures of those real eigenvalues (indicated by colors in the figure) and found them indeed opposite, in agreement with Theorem 4.

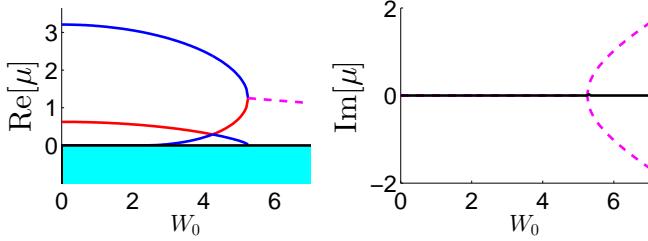


FIG. 1: Eigenvalues  $\mu$  for varying gain-loss strength  $W_0$  in the Scarff-II potential (2.3) with  $V_R = 5$  (the continuous spectrum is displayed in light blue). Blue lines indicate eigenvalues with positive  $\mathcal{PT}$ -Krein signatures while red lines indicate eigenvalues with negative  $\mathcal{PT}$ -Krein signatures. Complex eigenvalues are indicated with dotted purple lines.

Interestingly, Fig. 1 also shows another collision of simple real eigenvalues of opposite  $\mathcal{PT}$ -Krein signatures at  $W_0 = 4.25$  (which creates another exceptional point). However, after collision these real eigenvalues re-emerge and no complex eigenvalues bifurcate out. This shows that collision of real eigenvalues of opposite  $\mathcal{PT}$ -Krein signatures is a necessary but not sufficient condition for complex-eigenvalue bifurcation. A sufficient condition for complex-eigenvalue bifurcation can be found in later text [i.e.,  $\alpha \neq 0$ , see the paragraph below Eq. (4.12)]. This condition is not met at the other exceptional point, thus we do not see phase transition there.

#### IV. REDUCED MODEL NEAR PHASE TRANSITION

In this section, we consider the potential nonlinear Schrödinger equation (2.1) and analyze its solution dynamics near phase transition.

Let us suppose the  $\mathcal{PT}$ -symmetric potential in Eq. (2.1) takes the form

$$V(x; \epsilon) = V_0(x) + \epsilon^2 V_2(x), \quad (4.1)$$

where  $0 < \epsilon \ll 1$ . Here  $V_0(x)$  is the unperturbed potential,  $V_2(x)$  is the form of potential perturbation, and  $\epsilon^2$  is the strength of this perturbation. We assume that the unperturbed potential  $V_0(x)$  is at phase transition and possesses an exceptional point at  $\mu = \mu_0$ , i.e., the linear operator  $\partial_{xx} + V_0(x)$  has a single eigenfunction  $u_e(x)$  and a generalized eigenfunction  $u_g(x)$  at  $\mu_0$ . Defining

$$L_0 \equiv \partial_{xx} + V_0(x) + \mu_0, \quad (4.2)$$

then we have

$$L_0 u_e = 0, \quad L_0 u_g = u_e. \quad (4.3)$$

Since  $L_0$  is  $\mathcal{PT}$ -symmetric, both  $u_e$  and  $u_g$  can be chosen to be  $\mathcal{PT}$ -symmetric as well, i.e.,

$$u_e^*(-x) = u_e(x), \quad u_g^*(-x) = u_g(x). \quad (4.4)$$

By taking the complex conjugate of the  $L_0 u_e = 0$  equation, we see that  $u_e^*$  is in the kernel of the adjoint operator  $L_0^*$ . Thus the solvability condition for the  $L_0 u_g = u_e$  equation is that

$$\int_{-\infty}^{\infty} u_e^2 dx = 0. \quad (4.5)$$

In principle, an exceptional point can have algebraic multiplicities higher than two, meaning that it can have additional generalized eigenfunctions beside  $u_g$ . But in a generic case, an exceptional point is formed by the collision of two simple real eigenvalues, in which case its algebraic multiplicity is only two. For simplicity, we only consider such generic exceptional points in this article. Since their algebraic multiplicities are two, they do not admit other generalized eigenfunctions, i.e., the equation

$$L_0 u_{g2} = u_g$$

admits no localized solutions for  $u_{g2}$ . Since  $u_e^*$  is in the kernel of the adjoint operator  $L_0^*$ , the Fredholm condition on the above equation is that its right side be not orthogonal to  $u_e^*$ , i.e.,

$$D \equiv \int_{-\infty}^{\infty} u_e u_g dx \neq 0. \quad (4.6)$$

In addition, since  $u_e$  and  $u_g$  are  $\mathcal{PT}$ -symmetric, so is  $u_e u_g$ , hence  $D$  is real.

If the potential  $V_0(x)$  is perturbed to be (4.1), we study nonlinear dynamics in this perturbed potential by multi-scale perturbation methods below. First we expand the solution to Eq. (2.1) into a perturbation series,

$$\psi(x, z) = (\epsilon u_1(x, Z) + \epsilon^2 u_2 + \epsilon^3 u_3 + \dots) e^{-i\mu_0 z}, \quad (4.7)$$

where  $Z = \epsilon z$ . Then up to order  $\epsilon^3$  we have a system of equations

$$\begin{aligned} L_0 u_1 &= 0, \\ L_0 u_2 &= -i u_1 Z, \\ L_0 u_3 &= -i u_2 Z - V_2 u_1 - \sigma |u_1|^2 u_1. \end{aligned}$$

Since  $u_e^*$  is in the kernel of the adjoint operator  $L_0^*$ , the solvability conditions for these equations are that their right sides be orthogonal to the adjoint homogeneous solution  $u_e^*$ .

At orders  $\epsilon$  and  $\epsilon^2$  we find from (4.3) that

$$u_1 = A(Z) u_e(x), \quad (4.8a)$$

$$u_2 = -i A_Z u_g. \quad (4.8b)$$

At order  $\epsilon^3$  we have

$$L_0 u_3 = -A_{ZZ} u_g - AV_2 u_e - \sigma |A|^2 A |u_e|^2 u_e.$$

The solvability condition of this equation is

$$A_{ZZ} - \alpha A + \sigma_1 |A|^2 A = 0, \quad (4.9)$$

where

$$\alpha = -\frac{1}{D} \int_{-\infty}^{\infty} V_2 u_e^2 dx, \quad \sigma_1 = \frac{\sigma}{D} \int_{-\infty}^{\infty} |u_e|^2 u_e^2 dx. \quad (4.10)$$

Equation (4.9) for the wave envelope  $A(Z)$  is our reduced model for nonlinear wave dynamics near an exceptional (phase-transition) point. Since  $V_2$  and  $u_e$  are  $\mathcal{PT}$ -symmetric and  $D$  real,  $\alpha$  and  $\sigma_1$  are real.

The reduced model (4.9) is a fourth-order dynamical system since  $A$  is complex. However it has two conserved quantities,

$$I_1 = |A_Z|^2 - \alpha |A|^2 + \frac{\sigma_1}{2} |A|^4, \quad (4.11)$$

and

$$I_2 = A^* A_Z - A A_Z^*, \quad (4.12)$$

where  $dI_k/dZ = 0$  ( $k = 1, 2$ ). Due to these two conserved quantities, solution dynamics in Eq. (4.9) is confined to a two-dimensional surface, thus this dynamics cannot be chaotic. When  $Z \rightarrow \infty$ , the solution  $A$  can only approach a fixed point, or a periodic orbit, or infinity (if  $\sigma_1 > 0$ , infinity is further forbidden due to conservation of  $I_1$ ).

The parameter  $\alpha$  plays an important role in Eq. (4.9). Let us consider the small-amplitude limit ( $|A| \ll 1$ ), in which case Eq. (4.9) reduces to  $A_{ZZ} - \alpha Z = 0$ . If  $\alpha < 0$ , these infinitesimal (linear) modes are bounded, meaning that the system is below phase transition. But, if  $\alpha > 0$ , these linear modes exponentially grow, indicating that the system is above phase transition. Recall that  $\alpha$  is dependent on the potential perturbation  $V_2$ . Thus whether the perturbed potential is above or below phase transition depends on the sign of  $\alpha$ . In addition, the value of  $\alpha$  also determines whether or not the underlying exceptional point  $\mu = \mu_0$  is a phase-transition point: if  $\alpha \neq 0$ , then  $\mu = \mu_0$  is a phase-transition point; if  $\alpha = 0$ , then the answer is not certain, and further analysis is needed in order to determine whether  $\mu = \mu_0$  is a phase-transition point or not.

In the next two sections, we will describe the predictions of the reduced model (4.9) and compare them with the full system (2.1). In all our numerical comparisons, we will use the Scarff-II potential (2.3) with  $V_R = 2$ . At this  $V_R$  value, an exceptional point occurs when

$$W_0 = 2.25, \quad \mu_0 \approx -0.3144, \quad (4.13)$$

and this exceptional point is a phase-transition point. In the format (4.1) of the perturbed potential, this Scarff-II potential has

$$V_0(x) = 2 \operatorname{sech}^2(x) + i 2.25 \operatorname{sech}(x) \tanh(x), \quad (4.14a)$$

$$V_2(x) = i c \operatorname{sech}(x) \tanh(x). \quad (4.14b)$$

This potential is above phase transition when  $c = 1$  and below phase transition when  $c = -1$ . At this phase-transition point, the coefficients in the reduced model (4.9) are found to be

$$\alpha \approx 0.3144c, \quad \sigma_1 \approx 0.2700\sigma. \quad (4.15)$$

For these coefficients the eigenfunction  $u_e(x)$  has been normalized to have unit amplitude. In all our comparisons, we take  $\epsilon = 0.2$ . This  $\epsilon$  is not very small, but predictions of the reduced model (4.9) still match those in the full system (2.1) as we will see below.

## V. SOLUTION BEHAVIORS ABOVE PHASE TRANSITION

Our main interest is to investigate nonlinear wave dynamics above phase transition ( $\alpha > 0$ ). Previous studies on nonlinear  $\mathcal{PT}$ -symmetric systems overwhelmingly focused on solution behaviors below phase transition, because it was argued that coherent structures such as solitons would be unstable above phase transition (at least in  $\mathcal{PT}$ -symmetric periodic potentials). We will show in this section that in  $\mathcal{PT}$ -symmetric localized potentials, stable solitons and robust oscillating nonlinear modes do exist above phase transition.

### A. Soliton families and their stability

First we consider soliton solutions, which correspond to constant-amplitude solutions in the reduced model (4.9). Specifically, constant-amplitude solutions of the form

$$A(Z) = A_0 e^{-i\mu_1 Z} \quad (5.1)$$

in Eq. (4.9) correspond to soliton solutions of the form

$$\psi = u(x) e^{-i(\mu_0 + \epsilon \mu_1)z} \quad (5.2)$$

in Eq. (2.1), where  $u(x) \approx \epsilon A_0 u_e(x)$  to leading order. In this  $A$ -formula,  $A_0$  will be made real positive from phase invariance. Substituting (5.1) into (4.9), we find  $\mu_1$  as

$$\mu_1 = \pm \sqrt{\sigma_1 A_0^2 - \alpha}, \quad (5.3)$$

where the quantity under the square root must be non-negative. This equation relates the propagation constant  $\mu_1$  to the soliton amplitude parameter  $A_0$ .

Since  $\alpha > 0$  above phase transition, solutions (5.3) exist only when  $\sigma_1 > 0$ . For the Scarff-II potential (4.14), this means that above phase transition, solitons can only exist under self-focusing nonlinearity ( $\sigma > 0$ ). The physical reason for the existence of these solitons comes from the nonlinear feedback. It is commonly known that a  $\mathcal{PT}$ -symmetric complex potential is above phase transition when the imaginary part of the potential (relative to the real part) is above a certain threshold. In the

current case, even though the linear potential  $V(x; \epsilon)$  is above phase transition, the nonlinearity-induced positive refractive index  $\sigma|\psi|^2$ , when added to this linear potential, enhances its real part, which makes its imaginary part relatively weaker. As a consequence, the nonlinearity transforms the effective potential from above phase transition to below phase transition [21].

Notice also from Eq. (5.3) that these solitons exist only above a certain amplitude (or power) threshold, which is

$$A_0^2 \geq \alpha/\sigma_1. \quad (5.4)$$

This means that the nonlinearity-induced positive refractive index must be strong enough in order to transform the effective potential from above to below phase transition. Consequently, these solitons do not bifurcate from linear modes of the potential. In addition, the two branches of these solutions [corresponding to the plus and minus signs in (5.3)] are connected at this amplitude threshold and thus belong to a single soliton family.

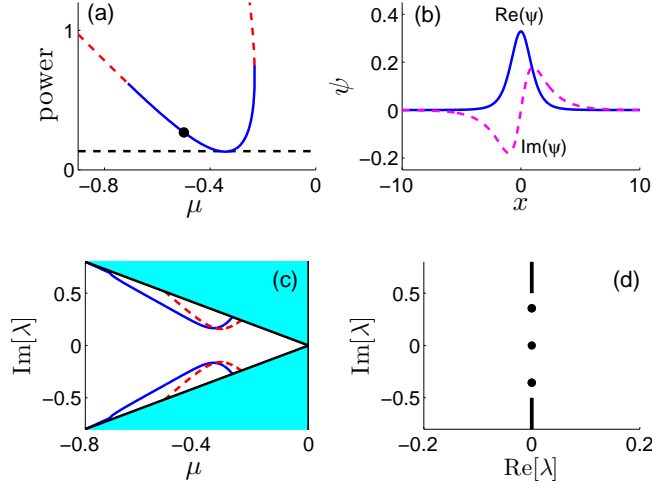


FIG. 2: (a) Power curve for the family of solitons above phase transition in the Scarff-II potential (4.14) with  $\sigma = 1$ ,  $c = 1$  and  $\epsilon = 0.2$ ; solid blue indicates stable solitons and dashed red unstable ones; the horizontal dashed line is the analytical prediction for the power minimum; (b) profile of an example soliton at the black-dot point of the power curve (where  $\mu = -0.5$ ); (c) discrete eigenvalues for stable solitons versus the propagation constant  $\mu$ ; solid blue are numerical values and dashed red analytical predictions; the shaded region is the continuous spectrum; (d) the numerically obtained linear-stability spectrum for the soliton in panel (b).

For the Scarff-II potential (4.14) with  $\sigma = 1$ ,  $c = 1$  and  $\epsilon = 0.2$ , we have numerically obtained these predicted solitons above phase transition, whose power curve is plotted in Fig. 2(a). Here the soliton's power is defined as  $P(\mu) = \int_{-\infty}^{\infty} |\psi|^2 dx$ . It is seen that this numerical power curve indeed has a minimum threshold. The analytical prediction for this power threshold, obtained from Eq. (5.4) and the leading-order perturbation solution (4.7)

as

$$P_{min} = \frac{\alpha \epsilon^2}{\sigma_1} \int_{-\infty}^{\infty} |u_e|^2 dx,$$

is also depicted in Fig. 2(a) (as a horizontal dashed line). It is seen that this analytical power threshold matches the numerical value very well. At the black-dot point of the numerical power curve (where  $\mu = -0.5$ ), the profile of the corresponding soliton solution is illustrated in Fig. 2(b). This soliton is  $\mathcal{PT}$ -symmetric, as are all other solitons in this family.

Stability of these solitons can be analyzed by examining the stability of constant-amplitude solutions (5.1) in the reduced ODE model (4.9). Let us perturb this constant-amplitude solution by normal modes as

$$A(Z) = \left( A_0 + \tilde{A} e^{\lambda_A Z} + \tilde{B}^* e^{\lambda_A^* Z} \right) e^{-i\mu_1 Z},$$

where  $\tilde{A}, \tilde{B} \ll 1$ , and  $\lambda_A$  is the eigenvalue from the envelope equation. Plugging this into (4.9) and linearizing, we obtain

$$L_A \begin{pmatrix} \tilde{A} \\ \tilde{B} \end{pmatrix} = 0,$$

where

$$L_A = \begin{pmatrix} \lambda_A^2 - 2i\lambda_A\mu_1 + \mu_1^2 + \alpha & \mu_1^2 + \alpha \\ \mu_1^2 + \alpha & \lambda_A^2 + 2i\lambda_A\mu_1 + \mu_1^2 + \alpha \end{pmatrix}.$$

Requiring the determinant of this matrix  $L_A$  to vanish, non-zero eigenvalues  $\lambda_A$  are then derived as

$$\lambda_A = \pm i \sqrt{2(3\mu_1^2 + \alpha)}.$$

Since  $\alpha > 0$  above phase transition, this formula predicts a pair of purely imaginary discrete eigenvalues, indicating that the constant-amplitude solution (5.1) is stable in the ODE model (4.9). This implies that the soliton solution (5.2) is also stable in the original model (2.1). Taking into account the scaling  $Z = \epsilon z$ , an approximation for non-zero discrete eigenvalues of this soliton is

$$\lambda \approx \epsilon \lambda_A = \pm i \epsilon \sqrt{2(3\mu_1^2 + \alpha)}. \quad (5.5)$$

Numerically we have confirmed the stability of these solitons near phase transition. This is achieved by computing the linear-stability spectrum of these solitons by the Fourier-collocation method [32]. For example, for the soliton shown in Fig. 2(b), its linear-stability spectrum is displayed in Fig. 2(d). All eigenvalues in this spectrum are purely imaginary, indicating that the soliton is linearly stable. In addition, the pair of discrete imaginary eigenvalues in this spectrum correspond to those predicted analytically by formula (5.5). Similar computations are performed for other solitons, and their stability is indicated by solid blue lines on the power diagram of Fig. 2(a). Quantitative comparison between numerical

discrete imaginary eigenvalues and their analytical prediction (5.5) is made in Fig. 2(c), and reasonable agreement can be seen (even though  $\epsilon = 0.2$  is not small here).

At high powers, we find that these solitons above phase transition become linearly unstable, and this instability is shown on the power curve of Fig. 2(a) by dashed red lines. The instability on the left side of the power curve is induced by complex-eigenvalue bifurcations from edges of the continuous spectrum, while instability on the right side of the power curve is caused by complex-eigenvalue bifurcations from interiors of the continuous spectrum. These high-power solitons correspond to amplitude values on the order  $A \sim 1/\epsilon$  and lie outside the validity of our perturbation theory, thus their instability does not contradict our stability result for low-power solitons.

## B. Oscillating solutions

The behavior of solutions away from the soliton equilibria can be largely captured by focusing on the case where  $A$  is purely real in the reduced system (4.9). In this case, the model equation becomes a simple second order ODE which we analyze using phase portraits. Above phase transition,  $\alpha > 0$ , this breaks into two cases depending on the sign of the nonlinearity.

### 1. Positive $\sigma_1$

In this case, the phase portrait is shown in Fig. 3(a), where  $\alpha$  and  $\sigma_1$  values are taken from Eq. (4.15) with  $c = 1$  and  $\sigma = 1$  (focusing nonlinearity). This phase portrait contains three fixed points. One of them is the origin, which is unstable, signifying that the system is above phase transition. The other two fixed points are at  $A = \pm\sqrt{\alpha/\sigma_1}$ , which are stable, and they correspond to the soliton of minimum power (with  $\mu_1 = 0$ ) in Eqs. (5.3)-(5.4). Away from these fixed points, the phase portrait features two types of periodic orbits which are separated by a figure-eight trajectory joined at the origin. Inner periodic orbits surround the non-zero fixed points, while outer periodic orbits undergo wider amplitude swings.

These periodic orbits in the phase plane imply the existence of robust oscillating solutions away from solitons in the full PDE (2.1), and such oscillating solutions are confirmed in our direct evolution simulations of that system. To illustrate, two examples of such PDE solutions are displayed in Fig. 3(b,c). Oscillations in panel (b) are stronger, and they correspond to outer periodic orbits in the phase portrait (a). Oscillations in panel (c) are weaker, and they correspond to inner periodic orbits in the phase portrait. This solution correspondence can be made more explicit by projecting the PDE solution onto the phase plane. To do so, we recall the perturbation solution (4.7)-(4.8), which to order  $\epsilon^2$  gives

$$\psi(x, z) = [\epsilon A(Z)u_e(x) - i\epsilon^2 A'(Z)u_g(x)] e^{-i\mu_0 z}. \quad (5.6)$$

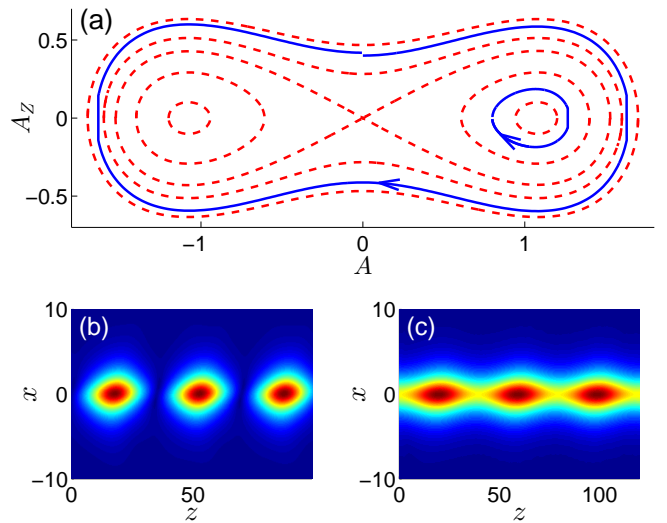


FIG. 3: (a) Phase portrait of the reduced model (4.9) with  $\sigma_1 > 0$  above phase transition. (b,c) Full PDE simulations in the Scarff-II potential (4.14) with  $\sigma = 1$ ,  $c = 1$  and  $\epsilon = 0.2$  under different initial conditions. In (a), solid blue lines are full PDE solutions in (b,c) projected onto the phase plane [with the outer curve for (b) and inner curve for (c)].

Taking the inner product of this equation with  $u_g(x)$  and retaining only the leading-order term, we get

$$A(Z) = \frac{1}{\epsilon D} \int_{-\infty}^{\infty} \psi(x, Z/\epsilon) u_g(x) dx e^{i\mu_0 Z/\epsilon}. \quad (5.7)$$

Taking the inner product of (5.6) with  $u_e(x)$  and recalling the relation (4.5), we get

$$A'(Z) = \frac{i}{\epsilon^2 D} \int_{-\infty}^{\infty} \psi(x, Z/\epsilon) u_e(x) dx e^{i\mu_0 Z/\epsilon}. \quad (5.8)$$

In this way, the full PDE solution can be embedded in the phase portrait of the ODE model for comparison. As a technical matter, the projected quantities  $(A, A')$  from the PDE solution by (5.7)-(5.8) are complex in general. But we have found that if the initial condition of the PDE solution is chosen according to Eq. (5.6), then the imaginary parts of the projected  $(A, A')$  remain very small for very long distances. Thus we neglect those small imaginary parts and plot only the real parts of the projected  $(A, A')$  in the phase plane.

For the two PDE solutions in Fig. 3(b,c), their phase-plane projections are displayed as solid blue lines in panel (a). It is seen that these PDE projections closely mimic the periodic orbits of the ODE model.

It is noted that these predictions of periodically-oscillating solutions in the PDE system are valid on the distance scale of  $z \sim 1/\epsilon$ . Beyond this distance scale, the PDE dynamics generally starts to deviate from the ODE predictions. Our numerics shows that over very long distances, these oscillations in the PDE solution gradually intensify and eventually break up, which is caused by res-



onance of nonlinearity-induced higher harmonics of these oscillations with the continuous spectrum in our opinion.

## 2. Negative $\sigma_1$

When  $\sigma_1 < 0$ , the phase portrait is shown in Fig. 4 (left panel), where  $\alpha$  and  $\sigma_1$  values are taken from Eq. (4.15) with  $c = 1$  and  $\sigma = -1$  (defocusing nonlinearity). In this case, except for the origin (an unstable fixed point), all trajectories escape to infinity. Similar solution behaviors are observed in the full PDE (2.1). An example is shown in the right panel of Fig. 4, where the PDE solution is seen to first decrease, and then rise to high amplitudes. The projection of this PDE solution onto the phase plane is displayed as a solid blue line in the phase portrait. This projection closely follows the trajectory of the ODE model. After the solution amplitude has reached the order  $A \sim 1/\epsilon$  (beyond the validity of our perturbation theory), PDE solutions can eventually saturate in amplitude while continuing to shed radiation and grow in power.

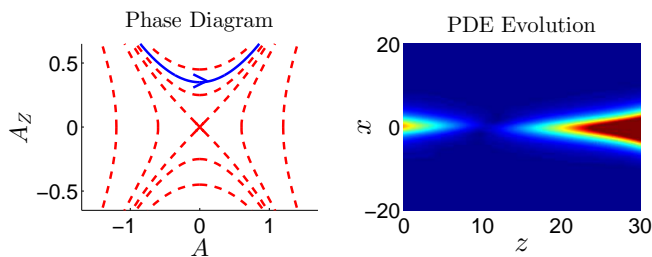


FIG. 4: (Left) Phase portrait of the reduced model (4.9) with  $\sigma_1 < 0$  above phase transition. (Right) Full PDE simulation in the Scarff-II potential (4.14) with  $\sigma = -1$ ,  $c = 1$  and  $\epsilon = 0.2$ . The solid blue line in the left panel is this full PDE solution projected onto the phase plane.

## VI. SOLUTION BEHAVIORS BELOW PHASE TRANSITION

In this section, we consider the predictions of our reduced model for solution behaviors below phase transition, and compare them with PDE solutions.

### A. Soliton solutions

Below phase transition,  $\alpha < 0$ , the ODE model (4.9) admits constant-amplitude solutions (5.1) for both signs of the nonlinear coefficient  $\sigma_1$ , meaning that solitons exist under both focusing and defocusing nonlinearities. But behaviors of solitons for the two signs of  $\sigma_1$  are very different.

When  $\sigma_1 > 0$ , formula (5.3), when rewritten as

$$A_0^2 = (\mu_1^2 + \alpha)/\sigma_1, \quad (6.1)$$

predicts that constant-amplitude solutions exist when  $|\mu_1| > \sqrt{|\alpha|}$ , i.e., soliton solutions exist when  $|\mu - \mu_0| > \epsilon\sqrt{|\alpha|}$ . In addition, the amplitude  $A_0$  (and hence power) of these solitons can be arbitrary. Numerically we have confirmed this prediction in the Scarff-II potential (4.14) with  $\sigma = 1$ ,  $c = -1$  and  $\epsilon = 0.2$ . The numerically obtained power curves of these solitons are displayed in Fig. 5(a). Stability of these solitons can be analyzed in the framework of the reduced model (4.9), and the eigenvalue formula (5.5) shows that these solitons are linearly stable, which agrees with the numerical findings in Fig. 5(a) for solitons at lower amplitudes (where the perturbation theory is valid). At higher amplitudes, the solitons do become unstable, similar to the case above phase transition in Fig. 2(a).

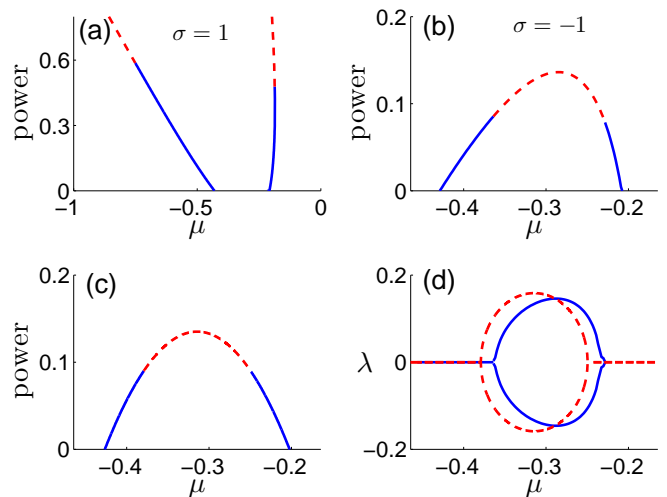


FIG. 5: (a,b) Numerically obtained power curves for the families of solitons below phase transition in the Scarff-II potential (4.14) with  $c = -1$ ,  $\epsilon = 0.2$ ,  $\sigma = 1$  in (a) and  $\sigma = -1$  in (b). (c) Analytical prediction for the power curve and linear stability of solitons in (b). In all of (a,b,c), solid blue indicates stable solitons and dashed red unstable ones. (d) Comparison of numerically obtained (solid blue) and analytically predicted (dashed red) unstable eigenvalues for solitons in (b).

When  $\sigma_1 < 0$ , formulae (5.3) and (6.1) predict that solitons only exist in the propagation-constant interval of  $|\mu - \mu_0| < \epsilon\sqrt{|\alpha|}$  with a limited range of amplitude values  $|A_0| \leq \sqrt{\alpha/\sigma_1}$ . The analytically predicted power curve from Eqs. (4.7), (4.8) and (6.1) is

$$P(\mu) \approx \frac{(\mu - \mu_0)^2 + \alpha\epsilon^2}{\sigma_1} \int_{-\infty}^{\infty} |u_e|^2 dx, \quad (6.2)$$

which is plotted in Fig. 5(c). Numerically we have obtained these solitons, whose power curve is shown in Fig. 5(b). This numerical power curve closely resembles the analytical prediction in (c). In particular, the existence of a power upper bound is confirmed. This close agreement between the perturbation theory and direct numerics is understandable, since these solitons have low



powers and are thus within the regime of validity of the perturbation theory.

The physical reason for limited power ranges of these solitons is that, under defocusing nonlinearity, if this power is too large, the negative nonlinearity-induced refractive index would transform the effective potential from below phase transition to above phase transition, rendering stationary solitons impossible.

Stability of these solitons with limited power ranges can be analyzed in the framework of the reduced model (4.9). In this case, the eigenvalue formula (5.5) predicts that these solitons are linearly unstable when

$$|\mu - \mu_0| < \epsilon \sqrt{|\alpha|/3}, \quad (6.3)$$

and stable otherwise. This predicted instability and stability is shown on the predicted power curve in Fig. 5(c). It is seen that solitons at the top part of the power curve are predicted as unstable and the bottom ones predicted as stable. Numerically we have determined the linear stability of these solitons by computing their stability spectra, and the results are shown in Fig. 5(b). Clearly the numerical results match those of analytical predictions. Quantitatively we have also computed real eigenvalues of unstable solitons and plotted them in Fig. 5(d), together with their analytical predictions in Eq. (5.5). This quantitative comparison shows good agreement as well.

### B. Oscillating solutions

Like the previous case above phase transition, robust oscillating solutions exist below phase transition as well. As before, we will unveil such solutions by focusing on the case of real  $A$  in the reduced model (4.9).

If  $\sigma_1 > 0$ , the phase portrait of the reduced model is shown in Fig. 6 (left panel), where  $\alpha$  and  $\sigma_1$  values are taken from Eq. (4.15) with  $c = -1$  and  $\sigma = 1$  (focusing nonlinearity). In this phase portrait the origin is a stable fixed point, a reflection that the system is below phase transition. Surrounding the origin are periodic orbits of various sizes. This implies an abundance of robust oscillating solutions in the PDE system. Numerically we have confirmed the existence of these oscillating solutions, and an example is shown in Fig. 6 (right panel). Projection of this PDE solution onto the phase plane is plotted as a solid blue line in the left panel, and good agreement with the ODE orbit is seen.

If  $\sigma_1 < 0$ , the phase portrait of the reduced model (4.9) is shown in Fig. 7(a), where  $\alpha$  and  $\sigma_1$  values are taken from Eq. (4.15) with  $c = -1$  and  $\sigma = -1$  (defocusing nonlinearity). This phase portrait contains three fixed points: the origin which is stable, and  $A = \pm\sqrt{\alpha/\sigma_1}$  which are unstable. The latter two fixed points correspond to the soliton with maximal power (at  $\mu = \mu_0$ ) in Fig. 5(c). Away from these three equilibria, trajectories are divided into two categories: periodic orbits surrounding the origin, and orbits which escape to infinity. Numerically we have found both types of solutions in the

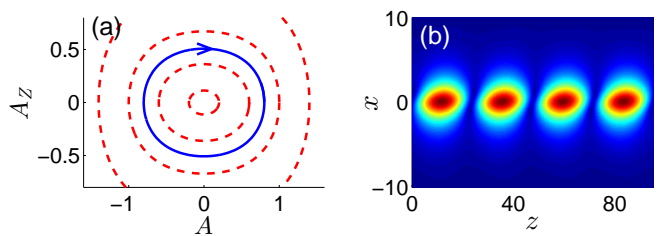


FIG. 6: (Left) Phase portrait of the reduced model (4.9) with  $\sigma_1 > 0$  below phase transition. (Right) Full PDE simulation in the Scarff-II potential (4.14) with  $\sigma = 1$ ,  $c = -1$  and  $\epsilon = 0.2$ . The solid blue line in the left panel is this full PDE solution projected onto the phase plane.

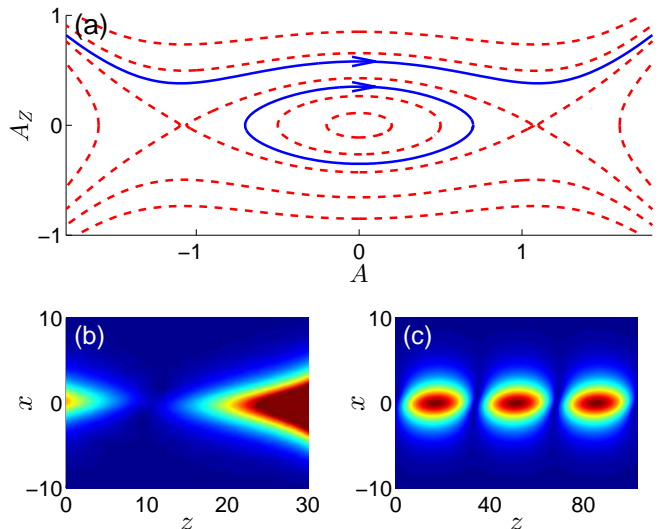


FIG. 7: (a) Phase portrait of the reduced model (4.9) with  $\sigma_1 < 0$  below phase transition. (b,c) Full PDE simulations in the Scarff-II potential (4.14) with  $\sigma = -1$ ,  $c = -1$  and  $\epsilon = 0.2$  under different initial conditions. In (a), solid blue lines are full PDE solutions in (b,c) projected onto the phase plane [with the upper curve for (b) and lower curve for (c)].

PDE system (2.1) under the Scarff-II potential (4.14) with  $\sigma = -1$ ,  $c = -1$  and  $\epsilon = 0.2$ , and two examples are displayed in Fig. 7(b,c). Projections of the PDE solutions onto the phase plane in panel (a) indicate that the ODE model accurately describes the PDE dynamics.

## VII. SUMMARY AND DISCUSSION

In this article, nonlinear wave propagation in  $\mathcal{PT}$ -symmetric localized potentials was investigated analytically near phase transition. Necessary conditions for phase transition were first derived based on a generalization of the Krein signature. Then rich nonlinear dynamics near phase transition was revealed through a multi-scale perturbation analysis, which yielded a nonlinear ODE model for the amplitude of the solutions. Above

phase transition, this ODE model predicted a family of stable solitons not bifurcating from linear modes under a certain sign of nonlinearity. In addition, it predicted persistent periodically-oscillating solutions away from solitons. Under the opposite sign of nonlinearity, it predicted unbounded growth of solutions. Below phase transition, solution dynamics was predicted as well. We have compared all analytical predictions with direct numerical calculations of the full PDE system and good agreement was obtained.

The analytical results obtained in this article are helpful for several reasons. First, it is known that phase transition is a distinct and important phenomenon in  $\mathcal{PT}$ -symmetric systems. Thus the analytical condition for phase transition in terms of  $\mathcal{PT}$ -Krein signatures helps understand when phase transition can or cannot occur. Second, the analytical predictions of nonlinear dynam-

ics near phase transition contribute to a global understanding of solution behaviors in  $\mathcal{PT}$ -symmetric systems. Thirdly, even though our analysis was performed only for the potential NLS equation (2.1), a similar treatment can obviously be extended to other  $\mathcal{PT}$ -symmetric systems near phase transition, and similar solution dynamics is expected in all such systems.

### Acknowledgment

This work was supported in part by the Air Force Office of Scientific Research (USAF 9550-12-1-0244) and the National Science Foundation (DMS-1311730).

- 
- [1] C.M. Bender and S. Boettcher, “Real spectra in non-Hermitian Hamiltonians having PT symmetry”, *Phys. Rev. Lett.* **80**, 5243–5246 (1998).
  - [2] R. El-Ganainy, K. G. Makris, D. N. Christodoulides and Z. H. Musslimani, “Theory of coupled optical  $\mathcal{PT}$ -symmetric structures,” *Opt. Lett.* **32**, 2632–2634 (2007).
  - [3] A. Guo, G.J. Salamo, D. Duchesne, R. Morandotti, M. Volatier-Ravat, V. Aimez, G.A. Siviloglou, and D.N. Christodoulides, “Observation of PT-Symmetry Breaking in Complex Optical Potentials”, *Phys. Rev. Lett.* **103**, 093902 (2009).
  - [4] C.E. Rueter, K.G. Makris, R. El-Ganainy, D.N. Christodoulides, M. Segev, and D. Kip, “Observation of parity-time symmetry in optics”, *Nature Phys.* **6**, 192-195 (2010).
  - [5] A. Regensburger, C. Bersch, M.A. Miri, G. Onishchukov, D.N. Christodoulides and U. Peschel, “Parity-time synthetic photonic lattices”, *Nature* **488**, 167-171 (2012).
  - [6] R. Driben and B.A. Malomed, “Stability of solitons in parity-time-symmetric couplers”, *Opt. Lett.* **36**, 4323 (2011).
  - [7] J. Schindler, A. Li, M. C. Zheng, F. M. Ellis, and T. Kottos, “Experimental study of active LRC circuits with PT symmetries,” *Phys. Rev. A* **84**, 040101(R) (2011).
  - [8] H. Cartarius and G. Wunner, “Model of a  $\mathcal{PT}$ -symmetric Bose-Einstein condensate in a  $\delta$ -function double-well potential”, *Phys. Rev. A* **86**, 013612 (2012).
  - [9] L. Feng, Y.L. Xu, W.S. Fegadolli, M.H. Lu, J.E.B. Oliveira, V.R. Almeida, Y.F. Chen, and A. Scherer, “Experimental demonstration of a unidirectional reflectionless parity-time metamaterial at optical frequencies”, *Nature Materials*, **12**, 108-113 (2013).
  - [10] C. M. Bender, B. Bertson, D. Parker, and E. Samuel, “Observation of PT Phase Transition in a Simple Mechanical System”, *Am. J. Phys.* **81**, 173179 (2013).
  - [11] B. Peng, S. Özdemir, F. Lei, F. Monifi, M. Gianfreda, G. Long, S. Fan, F. Nori, C. M. Bender, and L. Yang, “Paritytime-symmetric whispering-gallery microcavities”, *Nat. Phys.* **10**, 394 (2014).
  - [12] H. Hodaiei, M.-A. Miri, M. Heinrich, D. N. Christodoulides, M. Khajavikhan, “ $\mathcal{PT}$ -symmetric micro-ring laser”, *Science* **346**, 975-978 (2014).
  - [13] Z. Ahmed, “Real and complex discrete eigenvalues in an exactly solvable one-dimensional complex PT-invariant potential,” *Phys. Lett. A* **282**, 343 (2001).
  - [14] Z. H. Musslimani, K. G. Makris, R. El-Ganainy and D. N. Christodoulides, “Optical solitons in PT periodic potentials,” *Phys. Rev. Lett.* **100**, 030402 (2008).
  - [15] S. Nixon, L. Ge and J. Yang, “Stability analysis for solitons in  $\mathcal{PT}$ -symmetric optical lattices,” *Phys. Rev. A* **85**, 023822 (2012).
  - [16] F. K. Abdullaev, Y. V. Kartashov, V. V. Konotop, and D. A. Zezyulin, “Solitons in  $\mathcal{PT}$ -symmetric nonlinear lattices”, *Phys. Rev. A* **83**, 041805 (2011).
  - [17] M. Miri, A.B. Aceves, T. Kottos, V. Kovanis and D.N. Christodoulides, “Bragg solitons in nonlinear PT-symmetric periodic potentials”, *Phys. Rev. A* **86**, 033801 (2012).
  - [18] I.V. Barashenkov, S.V. Suchkov, A.A. Sukhorukov, S.V. Dmitriev, and Y.S. Kivshar, “Breathers in  $\mathcal{PT}$ -symmetric optical couplers”, *Phys. Rev. A* **86**, 053809 (2012).
  - [19] D. A. Zezyulin and V. V. Konotop, “Nonlinear Modes in Finite-Dimensional PT-Symmetric Systems”, *Phys. Rev. Lett.* **108**, 213906 (2012).
  - [20] P. G. Kevrekidis, D. E. Pelinovsky, and D. Y. Tyugin, “Nonlinear stationary states in PT-symmetric lattices”, *SIAM J. Appl. Dyn. Syst.* **12**, 1210 (2013).
  - [21] Y. Lumer, Y. Plotnik, M.C. Rechtsman, and M. Segev, “Nonlinearly induced PT transition in photonic systems”, *Phys. Rev. Lett.* **111**, 263901 (2013).
  - [22] J. Yang, “Symmetry breaking of solitons in one-dimensional parity-time-symmetric optical potentials”, *Opt. Lett.* **39**, 5547-5550 (2014).
  - [23] Z. Lin, H. Ramezani, T. Eichelkraut, T. Kottos, H. Cao and D.N. Christodoulides, “Unidirectional invisibility induced by  $\mathcal{PT}$ -symmetric periodic structures”, *Phys. Rev. Lett.* **106**, 213901 (2011).
  - [24] S. Nixon, Y. Zhu and J. Yang, “Nonlinear dynamics of wave packets in  $\mathcal{PT}$ -symmetric optical lattices near the

- phase transition point”, *Opt. Lett.* 37, 4874-4876 (2012).
- [25] S. Nixon and J. Yang, “Nonlinear dynamics of wave packets in  $\mathcal{PT}$ -symmetric optical lattices near the phase transition point”, *Opt. Lett.* 38, 1933-1935 (2013).
  - [26] M. Nazari, F. Nazari, and M. K. Moravvej-Farshi, “Dynamic behavior of spatial solitons propagating along Scarf II paritytime symmetric cells”, *J. Opt. Soc. Am. B* 29, 3057-3062 (2012).
  - [27] Shi, Z., X. Jiang, X. Zhu, and H. Li, “Bright spatial solitons in defocusing Kerr media with PT-symmetric potentials”, *Phys. Rev. A* 84, 053855 (2011).
  - [28] Chen, H., S. Hu, and L. Qi, “The optical solitons in the Scarff parity-time symmetric potentials”, *Opt. Commun.* 331, 139 (2014).
  - [29] R.S. MacKay, “Stability of equilibria of Hamiltonian systems,” in *Hamiltonian Dynamical Systems*, edited by R. S. MacKay and J. Meiss (Adam Hilger, Bristol), pp. 137-153 (1987).
  - [30] D.E. Pelinovsky, *Localization in Periodic Potentials: From Schrödinger Operators to the Gross-Pitaevskii Equation* (Cambridge University Press, Cambridge, UK, 2011).
  - [31] T. Kapitula and K. Promislow, *Spectral and Dynamical Stability of Nonlinear Waves* (Springer, New York, 2013).
  - [32] J. Yang, *Nonlinear Waves in Integrable and Nonintegrable Systems* (SIAM, Philadelphia, 2010).